Journal Pre-proofs

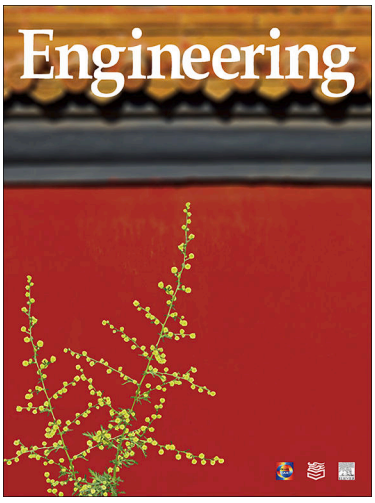

Article

Research on Fuel Cell Turboelectric Power Technology for Electric Aircraft

Yangjun Zhang, Ricardo Martinez-Botas, Zezhi Zeng, Andrew Jiaxuan Law, Hongsheng Jiang, Jie Peng, Dengjie Chen

PII: S2095-8099(26)00202-X
DOI: https://doi.org/10.1016/j.eng.2026.04.010
Reference: ENG 2325

To appear in: *Engineering*

Received Date: 29 May 2025
Revised Date: 2 April 2026
Accepted Date: 14 April 2026

Please cite this article as: Y. Zhang, R. Martinez-Botas, Z. Zeng, A.J. Law, H. Jiang, J. Peng, D. Chen, Research on Fuel Cell Turboelectric Power Technology for Electric Aircraft, *Engineering* (2026), doi: https://doi.org/10.1016/j.eng.2026.04.010

Research

Green Aviation Propulsion—Article

Research on Fuel Cell Turboelectric Power Technology for Electric Aircraft

Yangjun Zhang[a,*], Ricardo Martinez-Botas[b], Zezhi Zeng[a], Andrew Jiaxuan Law[b], Hongsheng Jiang[a], Jie Peng[c], Dengjie Chen[d]

[a]*School of Vehicle and Mobility, State Key Laboratory of Intelligent Green Vehicle and Mobility, Tsinghua University, Beijing 100084, China*

[b]*Sustainable Energy Technology and Turbomachinery Lab, Department of Mechanical Engineering, Imperial College London, London SW7 2AZ, UK*

[c]*Department of Engineering Mechanics, Tsinghua University, Beijing 100084, China,*

[d]*College of Chemistry and Materials Science, Jinan University, Guangzhou 510632, China*

*Corresponding author.

Email address: yjzhang@tsinghua.edu.cn (Y. Zhang)

Highlights

1. The fuel cell turboelectric power system is proposed for electric aircraft.
2. The proposed power system is more efficient for the cruise range larger than 300 km
3. The integration between fuel cell and combustor is demonstrated.
4. Outlet temperature of fuel cell combustor can reach 1200 ℃
5. A solid oxide fuel cell with a power density of 1.2W/g is manufactured.

Abstract

Electric aircraft will usher in a new era of low-altitude transportation and mark a third personalized transportation revolution. The power systems of electric aircraft must deliver ample power during takeoff and landing, operate at high efficiency during cruise, and exhibit high power density. Meeting all of these requirements is challenging for current power systems. We propose integrating fuel cells into the combustor of a conventional gas turbine to form a new fuel cell turboelectric power system for future electric aircraft. Its performance is compared with that of four other powertrains in a typical electric aircraft flight scenario through thermodynamic analysis. We demonstrate that the full Li-ion battery configuration remains suitable for short-range applications. In contrast, the fuel cell turboelectric power system is more efficient for medium- to high-range cruise requirements above 300 km. For a maximum cruising range of 500 km, the total equivalent hydrogen consumption of the fuel cell turboelectric power system is only 6.4 kg, approximately 50% of that of powertrains using conventional turbogenerators and batteries. Preliminary experiments are also conducted to validate the feasibility of developing a fuel cell turboelectric power system. The results demonstrate that a proton exchange membrane fuel cell can operate steadily with a flame combustor or a catalytic combustor. The outlet temperature of the fuel cell combustor can reach 1200 °C and is easily controlled by adjusting the gas flow rate to meet specific requirements. The power density of the manufactured finned tubular solid oxide fuel cell can also reach 1.2 $W \cdot g^{-1}$, thus meeting the requirements of future fuel cell turboelectric power systems. This study provides a technical and systematic foundation for the development of fuel cell turboelectric power systems.

Keywords

Fuel cell turboelectric power system, Electric aircraft, Aircars, Fuel cell, Combustion

1. Introduction

The invention of new power devices or transportation tools contributed significantly to the energy revolution. Steam trains and steam ships were invented during the first energy revolution, powered by coal-fired steam engines [1], whereas automobiles were invented during the second energy revolution, powered by internal combustion engines fueled by gasoline or diesel [2]. Electric aircraft powered by electricity or hydrogen are expected to prevail in future transportation, potentially initiating the third energy revolution. These electric aircraft mainly include electric vertical takeoff and landing (eVTOL) aircraft, also called aircars, which could be a widely accessible form of air transportation as commonplace as automobiles [3,4]. The demand for electrical power is expected to increase substantially as the electrification of the transportation sector advances. Improving the thermal efficiency and power density of the power systems for electric aircraft could effectively increase their flight range.

In general, a typical trip of an electric aircraft consists of five distinct phases: takeoff, climb, cruise, descent, and landing [5]. The power required for each phase varies significantly [6]. The instantaneous power needed for vertical takeoff is the greatest. More aerodynamic lift should be generated to overcome the air resistance and the weight of the electrical aircraft. The power demand during the cruise phase is the lowest, as vertical acceleration is no longer required. The power system for an aircraft should be well-adapted to the varying power demands at different phases of flight. To meet this requirement, the power system must deliver high power during take-off and landing and operate efficiently during cruise. A high power density is also required for a high payload [7].

The conventional power sources for aircraft are gas turbine engines [8,9], such as the widely used turboprop, turboshaft, and turbofan engines [10], which can continuously convert the thermal energy released during combustion into shaft work or thrust. The development of mobile power generation engines for electric aircraft requires careful consideration of integrating electronic components, such as electric motors and fuel cells, into the gas turbine system, thereby forming a turboelectric power system with high thermal efficiency and power density. The power is delivered as electricity via an electric motor rather than as mechanical shaft power via a turbine. The turboelectric power system is an electrified version of the conventional gas turbine engine.

Improving the motor's power density is crucial for the development of a turboelectric power system or turbogenerator [11]. The power densities of current motors cannot meet the goals of National Aeronautics and Space Administration (NASA)'s Advanced Air Transportation Technology Project [12]. The measured rated power of the current motors is lower than that of the electromagnetic design because dissipating the heat generated within the motor is difficult, leading to a significant temperature rise and potential structural failure. In previous studies, housing cooling [13], improved stator core cooling [14], improved winding cooling [15], and improved rotor cooling [16] were proposed to achieve proper thermal management of the motor and improve power density. Our group examined the effect of integrating heat pipes into the guide vane to transfer heat from the motor to the impeller's primary airflow, thereby increasing the motor power density to 4.8 $kW \cdot kg^{-1}$ under rated conditions [17]. The system's power density could therefore be substantially improved.

Improving the overall thermal efficiency of the power system is also very important and can be achieved by integrating fuel cell stacks into the gas turbine engine, as fuel cells can directly convert chemical energy into electricity with high efficiency [18,19]. There are two main types of fuel cells: proton-exchange membrane fuel cells (PEMFCs) and solid oxide fuel cells (SOFCs). PEMFCs initiate electrochemical reactions through a membrane-electrode assembly, where a Pt catalyst is used to lower the activation energy [18]. In contrast, SOFCs initiate an electrochemical reaction at a high operating temperature [20]. Most previous studies have focused on examining the effect of integrating SOFC stacks into gas turbine systems, as the operating temperature of an SOFC stack is approximately 800 °C, which is more compatible with the high working temperature of gas turbine engines than that of a PEMFC stack [21,22]. Fuel flexibility also enables SOFC stacks to operate with reformed hydrocarbons. However, because the development of current SOFC stacks has focused mainly on stationary power generation, their power density still needs further improvement for mobile power systems.

Conducting experimental studies on gas turbine engines integrated with SOFC stacks is also challenging [23,24]. Therefore, in most studies, primarily thermodynamic analyses of hybrid SOFC-gas turbine systems have been conducted. The overall thermal efficiencies, weights, and volumes of various hybrid systems have been calculated and evaluated [25,26]. In a previous study, a thermodynamic model was constructed to analyze the performance of turbojet and turbofan engines integrated with SOFC stacks and catalytic partial oxidation (CPOx) reactors. JP-5 was used as fuel, which was reformed to generate hydrogen and carbon monoxide. The thermal efficiency of the hybrid turbofan system increased by 8% because of the integration of SOFC stacks. The results of another related study also supported this finding [27]. Models were developed to assess the performance of a hybrid propulsion and power system incorporating fuel cells, with a focus on system efficiency and weight. A proper match among key components was emphasized to improve flight range. Variations in conditions can induce rapid changes in temperature distributions, potentially disrupting the system's thermal balance. Thus, precise regulation of working conditions is required for stabilization [28]. In one study, control strategies for SOFC-gas turbine systems were proposed to ensure robust operation across a wide range of dynamic thermal conditions [29]. NASA proposed designs of a 120 kW solid oxide fuel cell and gas turbine hybrid power system (SOFC-GT) for X-57 electric flight [30,31]. Their first design could achieve a fuel-to-electrical efficiency of 62% and a gravimetric power density greater than 0.3 $kW \cdot kg^{-1}$. However, this compact design requires the steady operation of the recycle blower at temperatures exceeding 900 °C, which is challenging for system development. The second design is not as compact as the first, but it could still achieve an efficiency of 55% and a power density of 0.281 $kW \cdot kg^{-1}$. NASA emphasized the importance of experimentally investigating the effect of integrating the fuel cell with the combustor [31]. They also reported that the most critical component of this system is its high-power-density fuel cell stack [23,32].

Unlike the traditional SOFC-GT system, which focuses primarily on improving the overall efficiency of the power system, a su and high efficiency during cruise. Appropriate power systems for future electric aircraft have been considered in very few studies. Moreover, most studies have only conducted thermodynamic analyses for different fuel cell gas turbine power systems. Parameter selection and component integration need further experimental investigation and validation. Only experiments can reveal the real challenges and validate the feasibility of developing such complicated power systems for future electrical aircraft.

In this article, we propose a new fuel cell turboelectric power system for future electric aircraft. Traditional SOFC-GT systems use primarily fuel cell stacks to deliver most of the power with high efficiency. Gas turbines are used for heat recovery, whereas we mainly modify the combustor in a conventional gas turbine system by incorporating fuel cell stacks. The power from the turbogenerator is approximately twice that of the fuel cell. This system differs from conventional SOFC-GT systems, whose main power is from SOFC stacks, which are generally connected with the gas turbine system in series [33]. We also tested the performance of integrating a PEMFC into a gas turbine system. This modification is based on the original high-power-density gas turbine power system and enables it to meet the high-efficiency, high-power-density requirements of electric aircraft. It is designed to deliver high power during takeoff and landing and to achieve high efficiency during the cruise phase. In our system, the fuel cell stacks can be connected to the gas turbine system either in series or in parallel.

In Section 2, the concept of the proposed power system is introduced. The performance of a typical flight profile for an electric aircraft is evaluated and compared with that of other conventional power systems. The challenges associated with developing a fuel cell turboelectric power system are also presented and discussed. In Section 3, experiments are presented to demonstrate the feasibility of power systems. In detail, the feasibility of integrating PEMFC stacks with combustors and manufacturing high-power-density tubular SOFCs is experimentally examined.

2. Fuel cell turboelectric power system

2.1 Schematic illustration of the proposed power system

The requirements for power systems in electric aircraft are greater than those for traditional cars and aircraft. High power output during take-off and landing, high efficiency during cruise, and high power density are all needed to achieve a practical flight range with a meaningful payload. A fuel cell turboelectric power system is proposed to meet the varying power demand of electric aircraft, as illustrated in Fig. 1. It can be regarded as a modification of the combustor for a conventional gas turbine system.

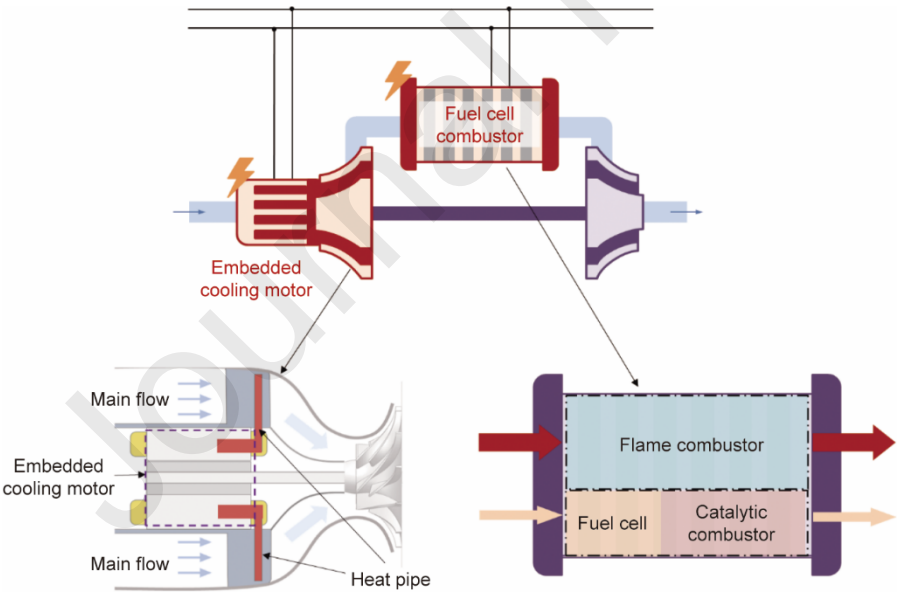

Fig. 1. Schematic illustration of the fuel cell turboelectric power system.

The fuel cell turboelectric power system is a hybrid system comprising an embedded cooling motor, a fuel cell combustor, and a gas turbine. During the take-off/landing phases, the gas turbine combustor is fully operational, and power is provided by the gas turbine system. During the cruise phase, the gas turbine combustor is deactivated, and the fuel cell is the primary power source for the electric aircraft. Under the rated condition, the power output from the gas turbine is approximately twice that from the fuel cells.

An embedded cooling motor is designed to increase the system power density [17]. The heat pipe is integrated into the motor guide vane to transfer heat generated inside the motor directly to the impeller's primary airflow. An increase in heat dissipation capacity could enable the motor to output more power, thereby improving its power density. The power density

of the embedded cooling motor under rated conditions can exceed 5 kW·kg^{-1}, which is highly beneficial for system dev

A fuel cell combustor is also proposed to improve the power system's thermal efficiency. A fuel cell is integrated into the combustor, as illustrated in Fig. 1. The fuel cell directly converts fuel energy into electricity with high efficiency. In contrast, the combustor can be used to increase the turbine inlet gas temperature. The fuel cell stacks used in the fuel cell combustor can be either PEMFC or SOFC stacks. Combining a fuel cell with a combustor is challenging, in part due to the mismatch between their required airflow rates and operating temperatures, especially for the PEMFC stack, which operates at only 60–80 °C. Generally, the airflow rate and operating temperature for fuel cell stacks are lower than those for the combustion chamber of a gas turbine.

To address these challenges, we develop a fuel cell combustor in two steps. The first step is to create a fuel cell combustor based on the PEMFC stack, as research and development on PEMFCs are more mature than on SOFCs. The feasibility of combining the fuel cell and combustor is first validated using the PEMFC stack. To increase system efficiency, fuel flexibility, and temperature compatibility of the fuel cell turboelectric power system, an SOFC stack is selected for the second stage of development. Various hydrocarbon fuels, such as kerosene, diesel, and gasoline, can be reformed into hydrogen and carbon monoxide for use in electrochemical reactions. This approach can circumvent the problems of hydrogen storage and transportation. However, the power density of the current SOFC stack is too low to meet power system requirements [31]. Increasing the power density of the SOFC stack before it is used to power electric aircraft is crucial. Preliminary experimental tests must be performed to validate the feasibility of achieving sufficient power density.

2.2 Comparisons among different power systems

In this study, the performance of power systems for typical electric aircraft is investigated, with a focus on eVTOLs. A representative trip of an eVTOL is illustrated in Fig. 2, which can be divided preliminarily into three phases: takeoff, cruising, and landing [34]. The takeoff phase consists of vertical ascent at a velocity of 20 km·h^{-1} until a cruising altitude of 1 km (~3280 ft (1 ft = 0.3048 m)) is reached. After that, the cruising phase involves horizontal travel at 250 km·h^{-1}, and the maximum cruising range is set as a variable. The travel speed, cruising altitude, and maximum cruising range are all carefully selected following early studies [35–37]. Finally, the vertical descent in the landing phase is similar to that in the take-off phase. The eVTOL was designed with a loaded airframe weight of 600 kg, which includes the airframe, passengers, and additional cargo. It features a lift-to-drag ratio of 10 during cruising.

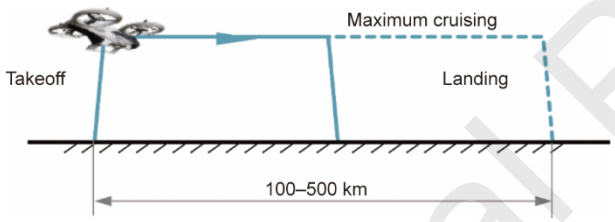

Fig. 2. Typical flight profile of an eVTOL.

The power requirements for each flight phase are based on the eVTOL's maximum take-off weight (MTOW). Moreover, the MTOW depends on the selected eVTOL powertrain configurations and the prescribed maximum cruising range. Range dependency is particularly important, as increasing range requirements imply greater fuel or battery weight required for the eVTOL. This increase has a cascading effect: the overall MTOW and the power and energy demand during cruising increase, which in turn further increases the weight requirements. This recursive relationship is considered when determining the MTOW of each powertrain system across a range of maximum cruising ranges from 100 to 500 km.

Schematic illustrations of the six different proposed powertrain configurations, which are the full Li-ion battery, the Li-ion battery and turbogenerator power system, the PEMFC and Li-ion battery power system, the SOFC and Li-ion battery power system, and the proposed fuel cell turboelectric power system with either the PEMFC or the SOFC combustor, are shown in Fig. 3. For the preliminary performance evaluation of the proposed eVTOL powertrains, the efficiencies and energy or power densities of the various powertrain components, along with the total efficiency of each power system, are listed in Table 1 [23,38–43]. Notably, the efficiencies and power densities of the turbogenerator and SOFC for the fuel cell turboelectric power system are based on the data collected in our early tests. The system efficiencies account for losses in the eVTOL's electric motor and transmission systems, both set to 0.92. The consumption of H_2 is determined by its lower heating value (LHV) of 120 MJ·kg^{-1}.

In addition, a portion of the MTOW accounts for the fuel/electrical energy required to be carried onboard the eVTOL. For electricity, this portion depends on the battery energy density, with current commercial electric vehicle (EV) packs having densities between 0.15 and 0.25 kW·h·kg^{-1} [38]. In contrast, for hydrogen, both the hydrogen fuel and the weight of the hydrogen storage system (such as the tank, casing, valves, sensors, and insulation) need to be considered. This dependence is expressed by the gravimetric storage efficiency, which ranges between 5% and 10% of the stored H_2 weight (wt% H_2) [44]. In this study, state-of-the-art values of 0.25 kW·h·kg^{-1} for Li-ion batteries and 10 wt% H_2 for hydrogen storage are used in the analysis, and the sensitivity effect of the storage weight assumptions is discussed.

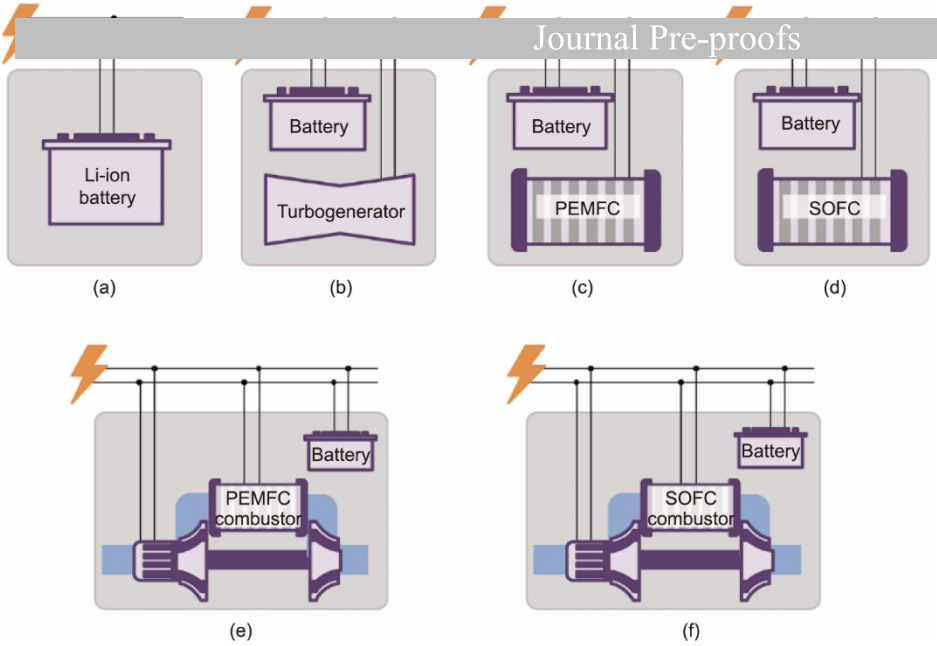

Fig. 3. Six potential powertrains for electric aircraft: (a) Li-ion battery power system, (b) Li-ion battery and turbogenerator power system, (c) PEMFC and Li-ion battery power system, (d) SOFC and Li-ion battery power system, (e) fuel cell turbo electric power system (PEMFC), and (f) fuel cell turbo electric power system (SOFC).

Table 1.
Performance metrics for eVTOL powertrain components [23,38–43]

Component	Component efficiency	System efficiency	Energy/power density
Li-ion battery	0.95	0.80	0.25 kW·h·kg^{-1}
Conventional turbogenerator	0.20	0.17	1.5 kW·kg^{-1}
PEMFC	0.45	0.38	0.7 kW·kg^{-1}
SOFC	0.60	0.51	1.0 kW·kg^{-1}

The power modules that operate different flight phases in each eVTOL powertrain are listed in Table 2. The powertrains are equipped with operating modes that correspond to the lowest-MTOW configuration and, consequently, the lowest energy consumption according to the metrics in Table 1, rather than adopting reverse operation. For the power system consisting of only a Li-ion battery and a turbogenerator, the battery is selected for cruise operation, while the turbogenerator is responsible for takeoff and landing. For the powertrains that contain a fuel cell system, the fuel cell is selected for cruise operation, whereas either the Li-ion battery or the turboelectric system manages takeoff and landing. The energy density is evaluated based on the flight profile at a cruising distance of 500 km and a cruising speed of 250 km·h^{-1}. For this flight mission, the power density of the fuel cell turboelectric power system (PEMFC) and the fuel cell turboelectric power system (SOFC) can reach 0.63 and 0.86 kW·kg^{-1}, respectively, meeting the power system requirements.

Table 2
eVTOL powertrain operating modes in each flight phase.

Powertrain	Takeoff/landing	Max. cruise	Energy density (kW·h·kg^{-1})
Full Li-ion battery	Li-ion battery	Li-ion battery	0.25
Li-ion battery and turbogenerator	Turbogenerator	Li-ion battery	0.35
Li-ion battery and PEMFC	Li-ion battery	PEMFC	0.60
Li-ion battery and SOFC	Li-ion battery	SOFC	0.79
Fuel cell turboelectric power system (PEMFC)	Turboelectric system	PEMFC	0.65
Fuel cell turboelectric power system (SOFC)	Turboelectric system	SOFC	0.88

Given that powertrains use a combination of energy sources, including H_2 gas and battery electricity, during flight, the total equi[Journal Pre-proofs]n the battery electricity consumption and the LHV of H_2 gas.

Finally, although this research focuses primarily on performance comparisons among potential eVTOL powertrain configurations, another essential consideration is the overall cost of each proposed powertrain. Given that the components are very different technologies, the cost can be broken down into the following factors:

- Component/system costs (capital expenditure (CapEx)) in production.
- Operating cost (OpEx) in terms of energy consumption (electricity and H_2) per kilometer.
- Durability costs for component degradation, maintenance and replacement over the eVTOL operating lifetime.
- Infrastructure costs for deploying energy refueling/recharging stations.

Analyzing the total cost requires separate, detailed, holistic analyses of the various cost factors to assess the feasibility of each eVTOL powertrain in full. Moreover, the ratio of the loaded airframe weight to the MTOW has been proposed as a secondary metric. This metric considers the weight of the airframe, passengers, and cargo, and compares them to the total weight of the eVTOL, serving as a proxy for the powertrain's cost-effectiveness. Finally, the powertrain's compactness is also taken into account. The airframe size is scaled according to higher MTOWs, which introduces a larger surface area (increasing drag) and volume (thereby further increasing the MTOW). Another optimal solution needs to be considered, and similarly, the ratio of the loaded airframe weight to the MTOW serves as a proxy for powertrain compactness.

The advantages and disadvantages of each powertrain configuration, in terms of quantitative vehicle performance metrics and qualitative cost comparisons, are summarized in Table 3.

Table 3
Summary of the advantages and disadvantages of eVTOL powertrain configurations.

Powertrain	Advantages	Disadvantages
Full Li-ion battery	Li-ion batteries have the highest component efficiency. Additional weight for fuel storage is required because it is an energy source. The overall infrastructure for electricity (battery production in USD·(kW·h)$^{-1}$ and charging grid) is more mature than that for H_2. Lower operating temperatures (< 60 °C) than those of fuel cell technologies provide better operational safety.	Because of the low energy density, full electric eVTOL operation is only suitable for short-to-medium range flights (< 300 km). Longer range flights lead to poorer energy consumption and higher costs, with large battery capacities introducing ineffective payload weight.
Li-ion battery and turbogenerator	Hybridization reduces the required Li-ion battery capacity and weight. Turbogenerators have higher power densities than fuel cells do. Turbocharging technology is long-established, operates safely, and has mature economies of scale.	Turbogenerators have the lowest component efficiency. Reduced battery capacity is offset by weight allocation for the H_2 storage system. Current H_2 infrastructure is immature.
Li-ion battery and PEMFC	Fuel cell technology has higher component efficiencies than turbogenerators do. Hybridization reduces the required Li-ion battery capacity and weight. Lower operating temperatures (60–80 °C) than those of SOFC provide better operational safety.	PEMFCs have lower component efficiency than SOFCs do and can only be powered by hydrogen. Reduced battery capacity is offset by weight allocation for the H_2 storage system. Current H_2 infrastructure is immature. Cold-start constraints for PEMFC stacks should be considered.
Li-ion battery and SOFC	SOFCs have higher component efficiencies and better compatibility with heat engines than PEMFCs do. Hybridization reduces the required Li-ion battery capacity and weight. SOFCs have better fuel flexibility and can use reformed hydrocarbons as fuel.	The thermal cycling reliability and lifespan of SOFCs need improvement. Reduced battery capacity is offset by weight allocation for the H_2 storage system. Current H_2 infrastructure is immature.
Fuel cell turbo electric power system (PEMFC)	The power density of a conventional turbogenerator is improved. Lower operating temperatures (60–80 °C) than those of SOFCs provide better operational safety.	PEMFCs have lower component efficiency than SOFCs do. Weight allocation is required for the H_2 storage system. Current H_2 infrastructure is immature.
Fuel cell turbo electric power system (SOFC)	The power density of conventional turbogenerators is improved. SOFCs have higher component efficiency and better fuel flexibility.	The thermal cycling reliability and lifespan of SOFCs need improvement. Weight allocation is required for H_2 storage systems. Current H_2 infrastructure is immature.

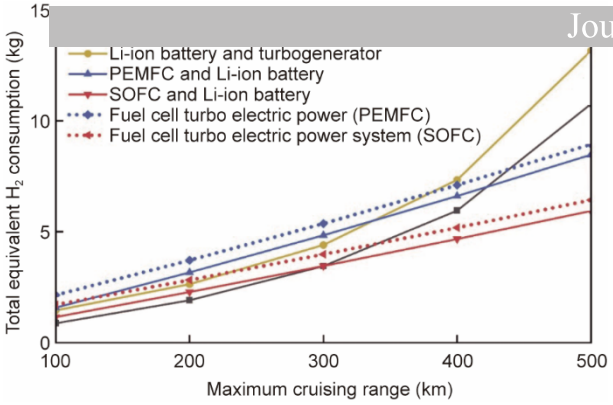

Fig. 4. Variations in total equivalent H_2 consumption with increasing maximum cruising range for the six proposed eVTOL powertrain configurations

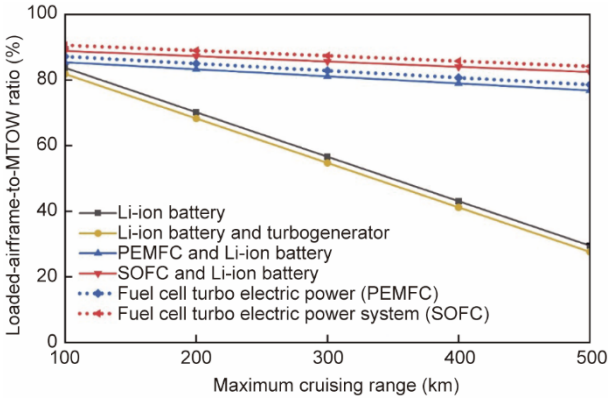

Fig. 5. Variations in the loaded-airframe-to-MTOW ratio with increasing maximum cruising range for the six proposed eVTOL powertrain configurations.

The total equivalent H_2 consumption for each mission profile and loaded-airframe-to-MTOW ratio is displayed in Figs. 4 and 5, respectively, for the six proposed eVTOL powertrains. Despite the low energy density of Li-ion batteries, the full Li-ion battery configuration is the best powertrain system for achieving maximum cruising ranges below 300 km, owing to its significantly higher component efficiency and the lowest equivalent H_2 consumption across all configurations. These findings indicate that full-electric operation is suitable for short-range applications, such as rapid urban air mobility via air taxis or short-distance travel. On the other hand, for maximum ranges exceeding 300 km, the full Li-ion battery configuration becomes less energy-efficient, as the additional battery weight outweighs its high efficiency. This is also reflected in its low loaded-airframe-to-MTOW ratio. This configuration also becomes unfeasible from a cost perspective, as battery capacities exceeding 100 kW·h are required for ranges of more than 300 km, and eVTOL sizing becomes less efficient. The use of a conventional generator (for takeoff and landing) with a Li-ion battery results in a less energy-efficient configuration for all cruising ranges because its component efficiency is significantly lower than that of both the Li-ion battery and H_2 fuel cell technology.

Powertrains that incorporate fuel cell technology offer more efficient options than the full Li-ion configuration for high maximum cruising range requirements, beginning with powertrains that combine Li-ion batteries and SOFCs, achieving over 300 km. The relationship between the total equivalent H_2 consumption and the maximum range is linear, and the loaded-airframe-to-MTOW ratio remains above 75%. Hence, fuel cell powertrains are more energy-efficient, cost-effective, and compact options for long-range eVTOL applications, such as intercity transportation. Powertrains that use SOFCs are superior to those that use PEMFCs because they have better component efficiency and energy density. These properties are beneficial provided that the high operating temperatures of the SOFCs are acceptable for safety in eVTOLs. Finally, compared with the SOFC turboelectric power system, the powertrain comprising a Li-ion battery and an SOFC has a slightly lower total equivalent H_2 consumption.

Acknowledging that the conducted analysis depends on the weight assumptions for both the Li-ion battery and the hydrogen storage system is essential. Using the lowest hydrogen gravimetric storage efficiency at 5 wt% H_2 (and 0.25 kW·h·kg^{-1} for the Li-ion battery), the cutoff point for the full Li-ion battery being the most energy-efficient powertrain increases slightly to 340 km, a 13% increase. On the other hand, when the lowest Li-ion battery energy density is 0.15 kW·h·kg^{-1} (and 10 wt% H_2 gravimetric storage efficiency), the cutoff point decreases significantly to just 175 km, which is a 41.7% reduction. Therefore, the battery energy density is most sensitive to the overall powertrain energy efficiency and, hence, to the suitability of H_2 fuel cell technology for different cruising ranges. Moreover, compared with the full Li-ion battery configuration, the hybridization of H_2 fuel cell technology with turboelectric power provides better loaded-airframe-to-MTOW ratios across all

cruising ranges. As such, even at shorter ranges (before the cutoff point), fuel cell turboelectric power systems might still be mor

Notably, the six proposed eVTOL powertrain configurations are compared using results from preliminary thermodynamic analysis. More detailed experimental investigations should be conducted in the future to account for the effects of system integration, power transmission, and safety factors. In this study, we first assess the feasibility of integrating fuel cells with the combustor in eVTOL powertrain applications, which is a crucial first step in system development.

3. PEMFC combustor

Integrating the PEMFC combustor into a conventional gas turbine engine to form a fuel cell turboelectric system could significantly improve overall system efficiency. PEMFCs can also be used during the takeoff/landing phases due to their faster startup capabilities. In our early test, we demonstrated that our PEMFC stack can achieve startup at a working temperature of −30 °C. Properly designing the hydrogen combustor of the PEMFC system is, therefore, extremely crucial for improving its performance and operational stability. The flow control and thermal management of the hydrogen combustor should be carefully considered. Two types of hydrogen combustion are incorporated into our design, as required by the system. They are flame combustion and catalytic combustion, respectively. Flame combustion could quickly increase the gas temperature and lead to a high outlet temperature of the PEMFC combustor, which could be used when large amounts of transient power are needed. In contrast, catalytic combustion is flameless and occurs at much lower gas temperatures; thus, it could be selected during the cruise phase.

3.1 Flame combustion

Flame combustion can rapidly increase the gas temperature, which typically results in high outlet temperatures. However, the combustion process is challenging to control, especially the rate of temperature rise, due to intense chemical reactions. We therefore convert large-scale flames into multiple microscale flames through micronozzles to control the flame combustion process. An image and a schematic illustration of the flame combustor developed in this study, made from the superalloy GH3625 and has a total length of 545 mm, are shown in Figs. 6(a) and (b), respectively. Hydrogen is injected through the micronozzles and mixed with the mainstream air for combustion. A schematic illustration of the microcombustion process and a detailed sectional view of the micronozzles are shown in Fig. 6(c) and (d), respectively. The micronozzles could lead to more uniform microscale fuel-lean combustion, thereby reducing both flame temperature and nitrogen oxide formation. During our preliminary test, the flame combustion could reach an outlet temperature of 1200 °C within 1 minute.

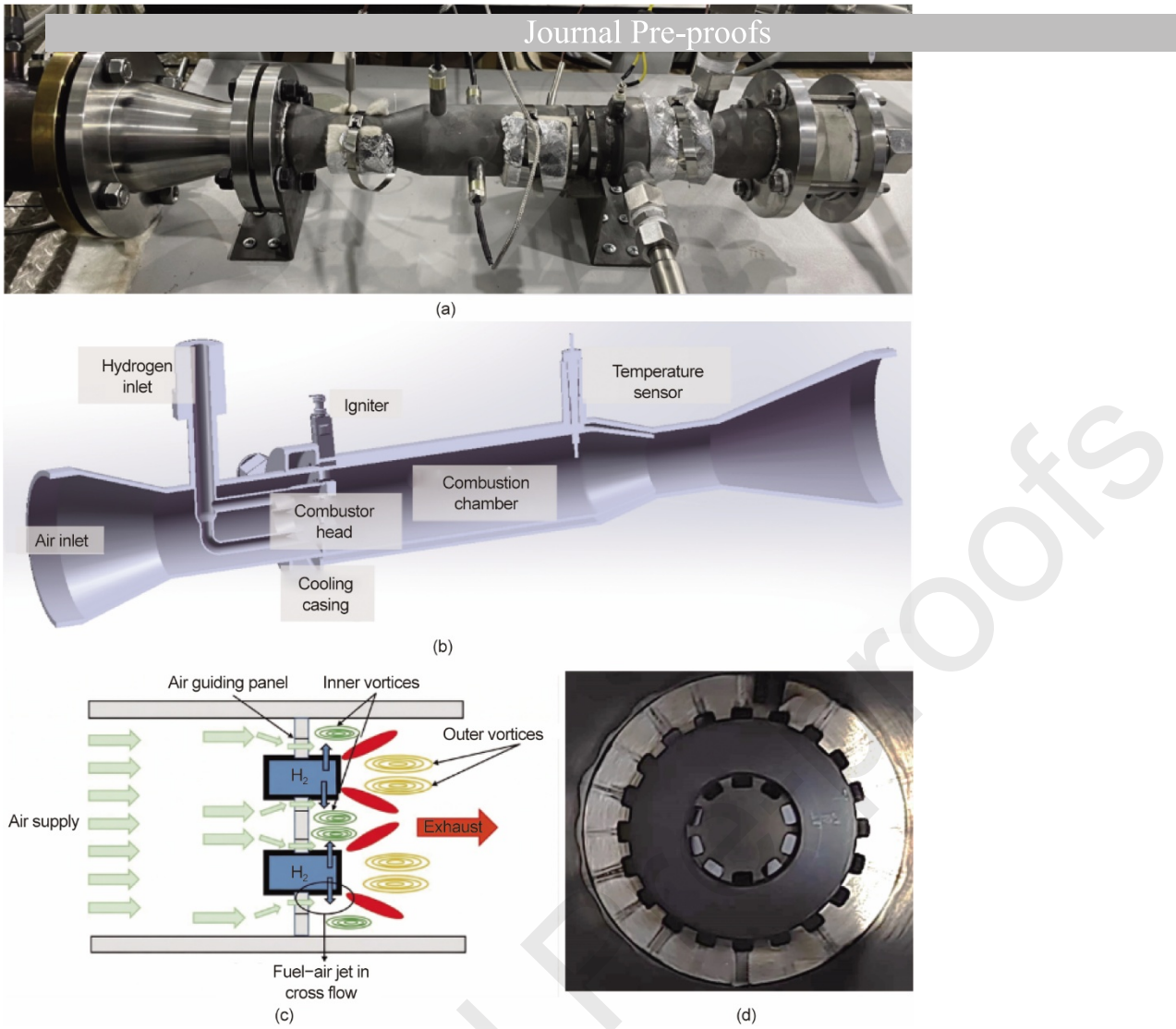

Fig. 6. (a) Image and (b) sectional view of the developed flame combustor. (c) Schematic illustration of the microcombustion process and (d) image of the micronozzles in the combustor.

A schematic illustration of the experimental setup used to test the performance of the PEMFC combustor using flame combustion in the present study is shown in Fig. 7(a). The effect of flame combustion was examined in this PEMFC combustor. Two streams of compressed hydrogen were fed to the PEMFC combustor. One stream was fed to the PEMFC stack for the electrochemical reaction, and the other stream was directly fed to the combustor. A mass flow meter with a range of 0–0.2 $g \cdot s^{-1}$ was used to measure the hydrogen flow rate, and a temperature sensor was placed at the inlet of the PEMFC stack to monitor the inlet temperature. Air was fed to the system, and its mass flow rate was measured by a mass flow meter with a range of 0–20 $g \cdot s^{-1}$. An electronic load was connected to the PEMFC stack to measure its output power. Three temperature sensors were placed at the combustor outlet to measure the gas temperature exiting the combustor.

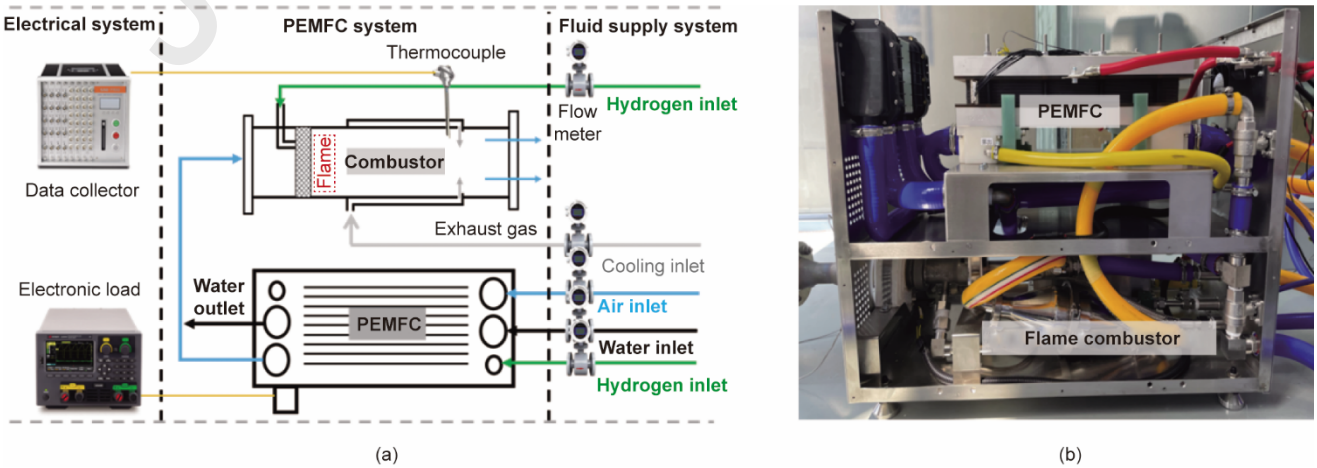

Fig. 7. (a) Schematic and (b) image of the examined PEMFC combustor

The developed PEMFC combustor used in our study is shown in Fig. 7(b). The PEMFC stack and the flame combustor are also illustrated. For each experimental run, the hydrogen and air were adjusted to the desired values and first fed to the PEMFC stack to ensure its stable operation. The mass flow rates of hydrogen and air were adjusted to 0.108 and 12.5 $g \cdot s^{-1}$, respectively, and the inlet temperature was fixed at 80 °C. Measurements were taken after the PEMFC stack began generating electricity. The temporal variation in the output power of the PEMFC stack is shown in Fig. 8(a). The stack power reached the desired value within approximately 3 min. As the output power stabilized to within 1%, another stream of hydrogen was fed into the flame combustor to initiate combustion. The outlet temperature of the gas exiting the combustor, measured by the three thermocouples, is shown in Fig. 8(b). The gas temperature increased from room temperature to 900 °C within around 20 seconds, then to 1200 °C within approximately 30 seconds. The outlet gas temperature was maintained at 1200 °C with a 1% variation, indicating reasonable control of the combustion process through the micronozzles. The fluctuation in the outlet gas temperature was approximately 20 °C, and its influence on the turbine efficiency was negligible. The PEMFC combustor could operate steadily, thus providing high-temperature gas to the turbine for large-scale power generation.

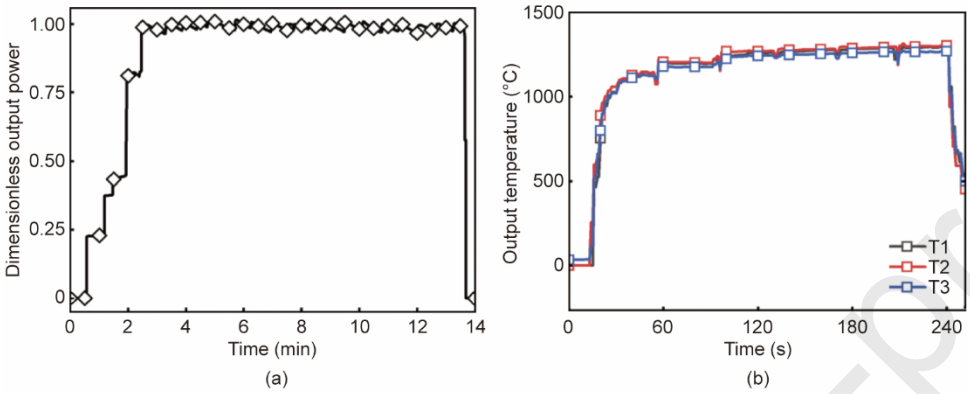

Fig. 8. Temporal variations in (a) the output power of the PEMFC combustor and (b) the outlet temperature of the PEMFC combustor. The results from all three thermocouples (T1–T3) at the outlet of the combustor are plotted.

3.2 Catalytic combustion

Catalytic combustion is flameless and easy to control. Hydrogen reacts with oxygen at the catalyst surface, reducing the activation energy of the reaction and enabling it to occur at a significantly lower temperature than in flame combustion. During this process, hydrogen and air are converted into water vapor, which releases heat and raises the gas temperature. In a typical catalytic combustor, the catalytic reaction of hydrogen and air cannot occur at a temperature of approximately 200 °C, which is 100 °C higher than the outlet gas temperature of the PEMFC stack. To initiate catalytic combustion under stack outlet conditions, bimetallic catalysts with favorable low-temperature performance are proposed to increase the gas temperature above 600 °C [45,46].

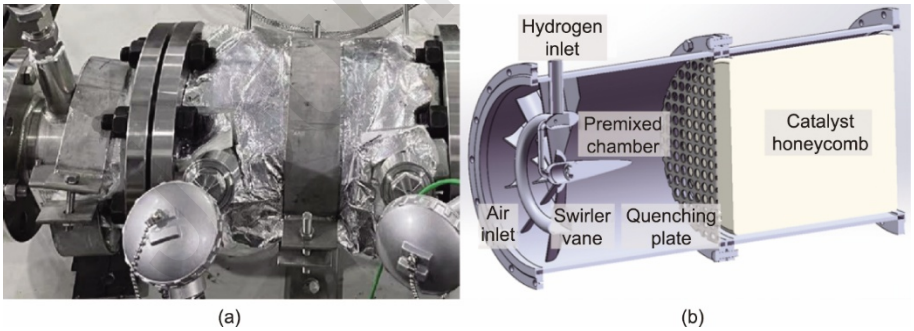

Fig. 9. (a) Image of the developed catalyst combustor and (b) sectional view of the catalyst combustor

A schematic illustration of the catalytic combustor, which consists mainly of two subchambers, one for gas premixing and another for catalytic combustion, where a catalytic core with bimetallic catalysts is loaded, is shown in Fig. 9. Thermal insulation flanges are added between these subchambers to mitigate the adverse effect of the heat released from the catalytic combustor. A tiny swirl generator is used to generate recirculation flows by mixing hydrogen and air in the subchamber. This design can achieve efficient mixing at a relatively low pressure loss. The mixed gas was then fed to the second subchamber for a catalytic reaction. The total length of the combustor is approximately 294 mm, and it is designed to increase the gas temperature to 600 °C. The outlet gas temperature of the catalytic combustor can be controlled by adjusting the mass flow rate of hydrogen or air.

A schematic illustration of the experimental setup used to test the performance of the PEMFC combustor with catalytic com…MFC stack and the catalytic combustor. The hydrogen mass flow rate was controlled by a flow meter with a range of 0–5 $g \cdot s^{-1}$. The air mass flow rate was controlled by a flow meter with a range of 0–600 $g \cdot s^{-1}$. A power regulator with a range of 0–200 kW was used to control and measure the output power of the PEMFC stack. Temperature sensors were placed at the outlet of the catalytic combustor to measure the outlet gas temperature. An image of the experimental setup constructed for performance testing is shown in Fig. 10(b).

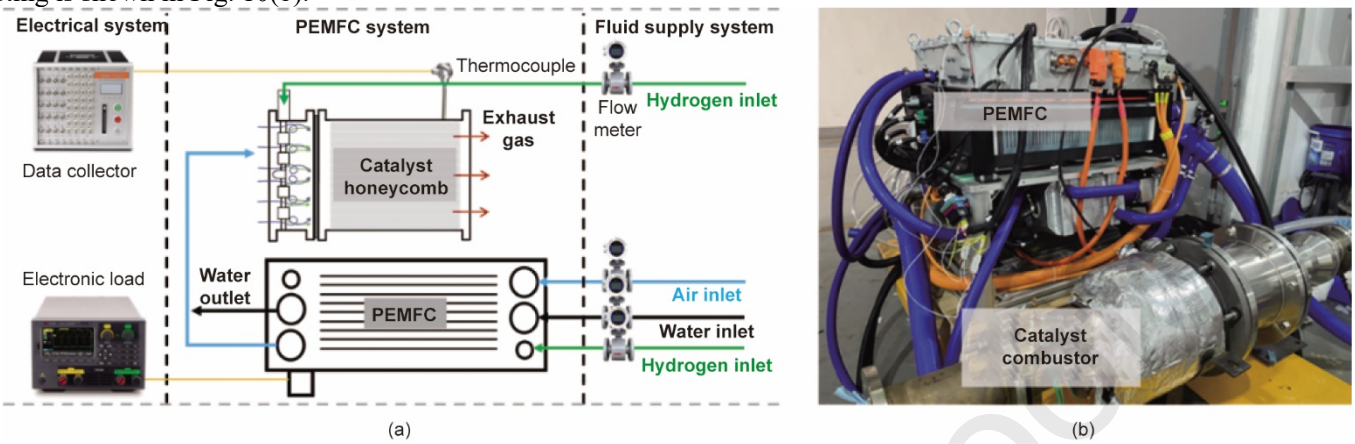

Fig. 10. (a) Schematic illustration of the experimental setup for testing the performance of the PEMFC combustor and (b) image of the PEMFC combustor.

The temporal variation in the output power of the PEMFC combustor is shown in Fig. 11. It took approximately 10 min for the PEMFC stack to reach the desired output power. As the power of the PEMFC stack stabilized within 1% for approximately 10 minutes, another stream of hydrogen was fed into the catalytic chamber for chemical reaction. The temporal variation in the outlet gas temperature in the combustor is shown in Fig. 11(b). For the first test, we set the target outlet temperature for the PEMFC combustor to 400 °C. The gas temperature in the catalytic combustor increases at a much lower rate than that in the flame combustor. The outlet gas temperature could increase from 100 to 400 °C within 10 min. The outlet temperature remained stable for 10 to 20 min, with negligible fluctuations.

For the second case, where the target outlet temperature was 600 °C, we adjusted the operating conditions to a higher hydrogen mass flow rate to examine its influence on the outlet temperature of the catalytic combustor. At a hydrogen mass flow rate of 3 $g \cdot s^{-1}$ and an air mass flow rate of 500 $g \cdot s^{-1}$, the outlet temperature of the combustor could reach 600 °C within approximately 10 min. Unlike the flame combustor, the catalytic reaction requires at least a few minutes to increase the gas temperature. However, compared with that of the flame combustor, the fluctuation in the gas temperature at the outlet of the catalytic combustor was significantly smaller. The PEMFC stack operated steadily during the outlet temperature adjustment, demonstrating good compatibility between the PEMFC stack and the catalytic combustor.

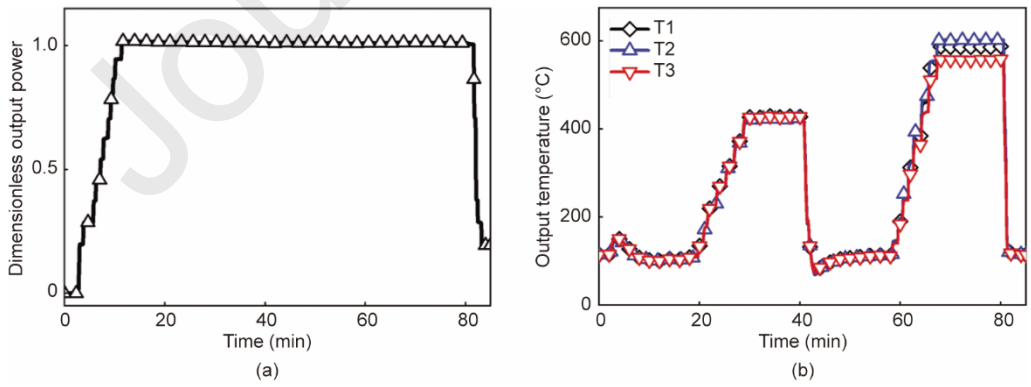

Fig. 11. Temporal variations in (a) the output power of the PEMFC combustor and (b) the outlet temperature of the PEMFC combustor. The results from all three thermocouples at the outlet of the combustor are plotted

4. Finned tubular SOFCs

Low power density has impeded the broader adoption of SOFC stacks in powering electric aircraft. Improving the gravimetric power density of SOFC stacks is crucial for the development of fuel cell turboelectric power systems, which determines whether this technology can be used [47]. The mismatch in reaction-rate limits between the anode and the cathode is the primary reason for the low power density of SOFC stacks. Because the reaction rate is proportional to the fuel concentration, cell temperature, and electrode specific surface area, a rigorous understanding of heat and mass transfer processes in SOFCs is essential for improving their gravimetric power density.

We propose a finned tubular SOFC to enhance local heat and mass transfer, thereby increasing the power density. The concept is illustrated in Fig. 12. The fin structure is inserted into the flow channels to induce radial flows, thereby increasing the fuel concentration at triple-phase boundaries. In our previous study, we demonstrated that the radial flow induced by the fin structure effectively increases power density by 20%–60% [48–50].

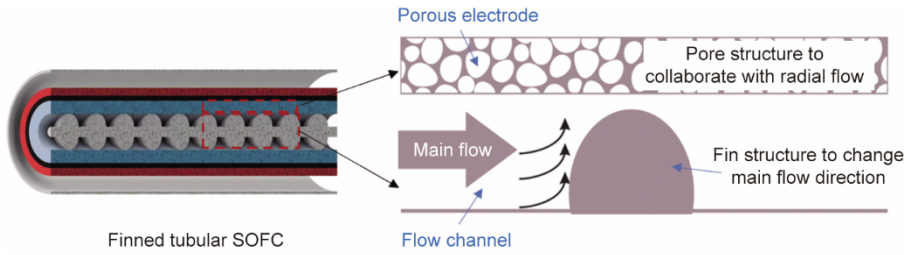

Fig. 12. Schematic illustration of a finned tubular SOFC.

To enhance the radial flow induced by the fin structure, the pore structure of the SOFC electrode should be carefully designed and optimized. The transfer phenomena and electrochemical activity in anode-supported SOFCs depend largely on the microstructure of the anode. In this section, we focus primarily on the effects of various pore structures on the gravimetric power density of tubular SOFCs. Traditional methods for preparing anode supports include mainly extrusion, dry pressing, and tape casting. However, these methods often yield an anode support with insufficient pores, as illustrated in Fig. 13(a), leading to significant resistance to gas transport. Many pore-forming agents, such as graphite and starch, are used to create extra pores within anodes after high-temperature sintering. Although the addition of pore-forming materials can effectively increase anode porosity, a large tortuosity factor remains, which is insufficient to promote gas diffusion. Low porosity and high tortuosity could lead to a nonuniform distribution of reactions.

To reduce gas transport resistance, we design a porous anode with ordered pores that increase porosity and decrease tortuosity, as illustrated in Fig. 13(b). Compared with traditional pores, ordered pores can direct gas diffusion from the flow channel to the triple-phase boundaries, resulting in significantly lower transport resistance. Pores of this type can facilitate mass transfer and increase both the local fuel concentration and the reaction rate within the porous anode, thereby increasing the power density. Increasing porosity could increase the number of straight, ordered pores, thereby lowering diffusion resistance and reducing weight. This increases output power while simultaneously reducing weight, hence increasing power density.

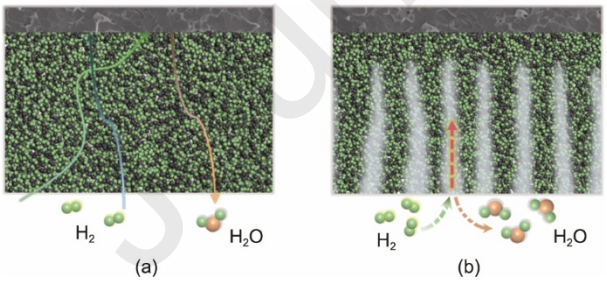

Fig. 13. Comparison between (a) traditional pores and (b) ordered pores

The ordered pores were manufactured using the phase inversion method, as shown in Fig. 14. An anode slurry that contained an electronic phase (e.g., NiO, which was later reduced to Ni) and an ionic phase (e.g., 8 mol% Y_2O_3-stabilized ZrO_2 (YSZ)) with an appropriate weight and particle size was prepared using ball milling with a liquid medium (e.g., ethanol). After the slurry was dried, the anode powder was obtained and ball-milled with plasticizers, solvents, and film-forming agents. The mixture was then placed in a vacuum to remove bubbles and passivated. To prepare a tubular structure, a clean glass rod with a specific diameter (e.g., 6 mm) was immersed in the passivated mixture and then pulled up, with the mixture adsorbed on its surface. This immersion and pulling process was repeated until the required thickness of the anode support was achieved. The coated rod was immersed in a container filled with deionized water for phase inversion. During this process, an ordered pore structure formed. The solidified tubular-shaped substrate was naturally demolded from the rod, followed by drying at a high temperature of approximately 1100 °C to burn out organic components and sinter the anode components for coating of the

electrolyte (e.g., YSZ), buffer layer (e.g., $Gd_{0.2}Ce_{0.8}O_{2-\delta}$), and cathode (e.g., $Ba_{0.5}Sr_{0.5}Co_{0.8}Fe_{0.2}O_{3-\delta}$) to form a single tubular fuel

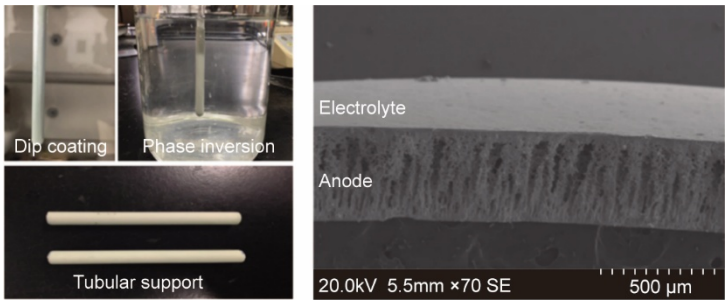

Fig. 14. Manufacturing process for the tubular SOFC with ordered pores

A schematic illustration of the experimental setup for testing the gravimetric power density of a tubular SOFC with ordered pores is shown in Fig. 15. The setup consists mainly of the tubular SOFC, a furnace, a thermocouple, a multimeter and a weight scale. The tubular SOFC, with a diameter of 6 mm and a length of 40 mm, was mounted in a furnace whose interior temperature can be adjusted from 20 to 850 °C. A thermocouple was placed inside the furnace to monitor the operating temperature of the tubular SOFC. The multimeter, which had a voltage range of 0–100 V and a current range of 0–7.35 A, was used to measure the output power of the tubular SOFC. The weight scale was used to measure the mass of the tubular SOFC. Because the experiment was conducted at high temperatures, a sensor was used to monitor the surrounding hydrogen concentration to ensure safety.

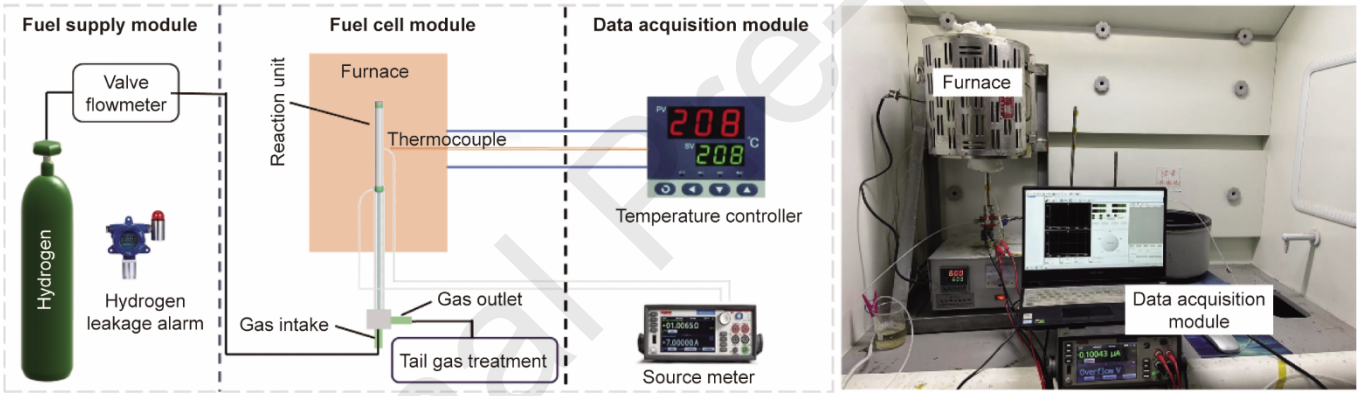

Fig. 15. Schematic illustration of the experimental setup of the tubular SOFC.

For each experimental run, compressed hydrogen was fed to the tubular SOFC at a flow rate of 40 mL·min^{-1}. The furnace was heated at a rate of 10 °C·min^{-1} until its temperature reached 400 °C. The hydrogen flow rate was then adjusted to 80 mL · min^{-1}, and the furnace heating rate was reduced to 5 °C · min^{-1} to prevent structural failure of the tubular SOFC. Measurements were taken when the temperature inside the furnace reached 750 °C and the variation in the open-circuit voltage was less than 0.01 V. During the measurement, we gradually increased the current load on the tubular SOFC and measured its operating voltage to plot the polarization curve.

The polarization curve of the tubular SOFC with ordered pores is compared with that of the traditional random pores in Fig. 16. The open-circuit voltages for both tubular SOFCs exceeded 1.0 V, which indicates that the manufactured 10 μm-thick electrolyte is dense and reliable and effectively prevents hydrogen on the anode side from mixing with oxygen on the cathode side. As shown in Fig. 16, the operating voltages of both tubular SOFCs decreased gradually as the current density increased. The polarization curve of the tubular SOFC with ordered pores has a lower rate of decrease than that of the traditional tubular SOFC, which indicates better electrochemical performance under the same working conditions. The high fuel concentration significantly increased the power density of the tubular SOFC with ordered pores at the triple-phase boundaries, facilitated by low gas-diffusion resistance. At an operating voltage of approximately 0.4 V, the gravimetric power density of the tubular SOFC with ordered pores reached 1.2 W·g^{-1}, approximately twice that of traditional tubular SOFCs, and meets the requirements for powering electric aircraft.

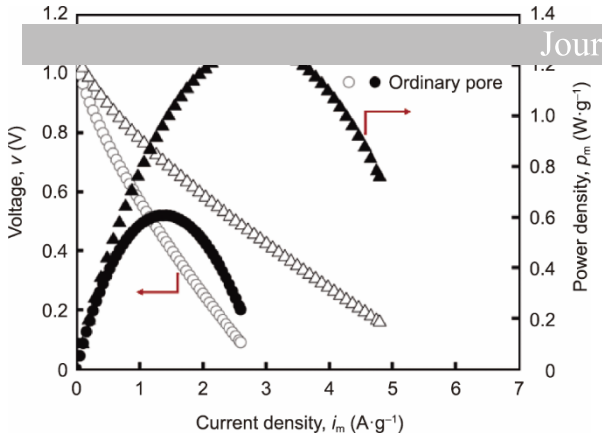

Fig. 16. Comparison of the voltages and power densities as functions of current densities for the tubular SOFC with ordinary pores (circles) and ordered pores (triangles).

Notably, the gravimetric power density of the tubular SOFC may decrease further as output power increases. A rigorous understanding of heat and mass transfer processes can help designers reduce the difference in reaction-rate limits between the anode and cathode, thereby improving the SOFC stack's gravimetric power density. In this study, we have demonstrated only the feasibility of manufacturing a high-power-density SOFC. Notably, developing an SOFC stack for a fuel cell turboelectric power system still requires careful experimental investigations to improve the long-term operational stability and thermal cycling reliability.

5. Conclusions

A fuel cell turboelectric power system for powering future electric aircraft is proposed. Preliminary thermodynamic analyses of six different powertrains were conducted. In detail, the total equivalent H_2 consumption and loaded-airframe-to-MTOW ratios for six power systems were determined for a typical eVTOL flight profile with cruising ranges from 100 to 500 km.

We showed that the full Li-ion battery configuration remains suitable for short-range applications. In contrast, the fuel cell turboelectric power system is more efficient for medium- to high-range cruise requirements above 300 km. For a maximum cruising range of 500 km, the total equivalent hydrogen consumption of the fuel cell turboelectric power system is only 6.4 kg, approximately 50% of that of conventional powertrains with turbogenerators and batteries. Notably, the preliminary comparison did not account for real system integration, safety design, or power transmission across all powertrains. More detailed analyses of real mission load profiles will be conducted in future studies.

In this study, we conducted preliminary experiments to assess the feasibility of developing a fuel-cell turboelectric power system. First, the feasibility of developing a PEMFC combustor was demonstrated. We showed that the PEMFC stack can operate steadily with both flame and catalytic combustors. The flame combustor outlet temperature can reach 1200 °C within 30 seconds. The outlet temperature of the catalytic combustor is lower than that of the flame combustor, but it is easier to control. Increasing the outlet temperature of the catalytic combustor from 400 to 600 °C within several minutes was also successful. The feasibility of manufacturing high-power-density SOFCs for the proposed power system was also demonstrated. A finned tubular solid oxide fuel cell was manufactured to improve electrochemical performance and reduce cell weight. The SOFC power density reached 1.2 W·g^{-1}, meeting the requirements of fuel cell turboelectric power systems.

Although the fundamental feasibility of developing a fuel cell turboelectric power system was demonstrated in this study, further experiments are required before a power system can be developed. For instance, experiments should be conducted to assess the performance of integrating a fuel cell combustor with a gas turbine system. The control system for monitoring the system's rapid dynamic response also requires testing. Structural design to avoid hydrogen accumulation inside the power system and to facilitate compact design should also be investigated. With respect to tubular solid oxide fuel cells, their long-term operation and thermal cycling reliability performance should be experimentally examined. The integration of the SOFC stack with the combustor may be easier than that of the PEMFC stack, but it should also be experimentally tested.

The present work aims to improve our understanding of the use of fuel cell turboelectric power systems for electric aircraft. It provides a foundation for the systematic design and optimization of electric aircraft powertrain systems.

Acknowledgments

This article is based on work supported in part by the National Natural Science Foundation of China (52507257) and the Independent Research Project of the State Key Laboratory of Intelligent Green Vehicle and Mobility, Tsinghua University (ZZ-PY-20250202 and ZZ-PY-20250203).

References

[1] Zou C, Zhao Q, Zhang G, Xiong B. Energy revolution: from a fossil energy era to a new energy era. Nat Gas Ind B 2016;3(1):1–11.
[2] Alagumalai A. Internal combustion engines: progress and prospects. Renew Sustain Energy Rev 2014;38:561–71.
[3] Liu M, Qian Y, Luo Y, Hao H, Liu Z, Zhao F, et al. Lifecycle greenhouse gas emissions and energy cost analysis of flying cars with three different propulsion systems. J Clean Prod 2022;331:129985.
[4] Swaminathan N, Reddy SRP, RajaShekara K, Haran KS. Flying cars and eVTOLs—technology advancements, powertrain architectures, and design. IEEE Trans Transp Electrif 2022;8(4):4105–17.
[5] Yang X, Liu T, Ge S, Rountree E, Wang C. Challenges and key requirements of batteries for electric vertical takeoff and landing aircraft. Joule 2021;5(7):1644–59.
[6] Luo Y, Qian Y, Zeng Z, Zhang Y. Simulation and analysis of operating characteristics of power battery for flying car utilization. eTransportation 2021;8:100111.
[7] Zhang Y, Qian Y, Zhuge WQ, Zhang L, Peng J, Xu B, et al. Progress and key technologies of flying cars. J Automot Saf Energy 2020;11(1):1–16. Chinese.
[8] Kauser F. An overview of gas turbine propulsion technology. In: Proceedings of the 30th Joint Propulsion Conference and Exhibit; 1994 Jun 27–29; Indianapolis, IN, USA. Reston: American Institute of Aeronautics and Astronautics; 1994.
[9] Aygun H. Effects of air to fuel ratio on parameters of combustor used for gas turbine engines: applications of turbojet, turbofan, turboprop and turboshaft. Energy 2024;305:132346.
[10] Dursun OO, Toraman S, Aygun H. Modeling of performance and thermodynamic metrics of a conceptual turboprop engine by comparing different machine learning approaches. Int J Energy Res 2022;46(15):21084–103.
[11] Dong C, Qian Y, Zhang Y, Zhuge W. A review of thermal designs for improving power density in electrical machines. IEEE Trans Transp Electrif 2020;6(4):1386–400.
[12] Jansen R, Bowman C, Jankovsky A. Sizing power components of an electrically driven tail cone thruster and a range extender. In: Proceedings of the 16th AIAA Aviation Technology, Integration, and Operations Conference; 2016 Jun 13–17; Washington, DC, USA. Reston: American Institute of Aeronautics and Astronautics; 2016.
[13] Ulbrich S, Kopte J, Proske J. Cooling fin optimization on a TEFC electrical machine housing using a 2-D conjugate heat transfer model. IEEE Trans Ind Electron 2018;65(2):1711–8.
[14] Lu Q, Zhang X, Chen Y, Huang X, Ye Y, Zhu ZQ. Modeling and investigation of thermal characteristics of a water-cooled permanent-magnet linear motor. IEEE Trans Ind Appl 2015;51(3):2086–96.
[15] Sun Y, Zhang S, Yuan W, Tang Y, Li J, Tang K. Applicability study of the potting material based thermal management strategy for permanent magnet synchronous motors. Appl Therm Eng 2019;149:1370–8.
[16] Fawzal AS, Cirstea RM, Gyftakis KN, Woolmer TJ, Dickison M, Blundell M. Fan performance analysis for rotor cooling of axial flux permanent magnet machines. IEEE Trans Ind Appl 2017;53(4):3295–304.
[17] Dong C, Hu X, Qian Y, Zhuge W, Zhang Y. Thermal management integrated with flat heat pipes for in-slot stator windings of electric motors. IEEE Trans Ind Appl 2023;59(1):699–711.
[18] Malik V, Srivastava S, Bhatnagar MK, Vishnoi M. Comparative study and analysis between Solid Oxide Fuel Cells (SOFC) and Proton Exchange Membrane (PEM) fuel cell – a review. Mater Today Proc 2021;47:2270–75.
[19] Zeng Z, Hao C, Zhao B, Qian Y, Zhuge W, Wang Y, et al. Local heat transfer enhancement by recirculation flows for temperature gradient reduction in a tubular SOFC. Int J Green Energy 2022;19(10):1132–47.
[20] Zeng Z, Qian Y, Zhang Y, Hao C, Dan D, Zhuge W. A review of heat transfer and thermal management methods for temperature gradient reduction in Solid Oxide Fuel Cell (SOFC) stacks. Appl Energy 2020;280:115899.
[21] Hao C, Zhao B, Essaghouri A, Qian Y, Zhuge W, Zhang Y, et al. A reduced-order electrochemical model for analyzing temperature distributions in a tubular solid oxide fuel cell stack. Appl Therm Eng 2023;233:121204.
[22] Hao C, Zeng Z, Zhao B, Qian Y, Zhuge W, Wang Y, et al. Local heat generation management for temperature gradient reduction in tubular solid oxide fuel cells. Appl Therm Eng 2022;211:118453.
[23] Cable TL, Sofie SW. A symmetrical, planar SOFC design for NASA's high specific power density requirements. J Power Sources 2007;174(1):221–7.
[24] Yuan Q, Li X, Han S, Wang S, Wang M, Chen R, et al. Performance analysis and optimization of SOFC/GT Hybrid systems: a review. Energies 2024;17(5):1265.
[25] Granovskii M, Dincer I, Rosen MA. Performance comparison of two combined SOFC–gas turbine systems. J Power Sources 2007;165(1):307–14.
[26] Waters DF, Pratt LM, Cadou CP. Gas turbine/solid oxide fuel cell hybrids for aircraft propulsion and power. J Propuls Power 2021;37(3):349–61.
[27] Ji Z, Rokni MM, Qin J, Zhang S, Dong P. Energy and configuration management strategy for battery/fuel cell/jet engine hybrid propulsion and power systems on aircraft. Energy Convers Manage 2020;225:113393.
[28] Harun NF, Tucker D, Adams II TA. Fuel composition transients in solid oxide fuel cell gas turbine hybrid systems for polygeneration applications. J Fuel Cell Sci Technol 2014;11(6):061001.
[29] Oh S, Sun J, Dobbs H, King J. Model predictive control for power and thermal management of an integrated solid oxide fuel cell and turbocharger system. IEEE Trans Control Syst Technol 2014;22(3):911–20.
[30] Papathakis KV, Schnarr OC, Lavelle TM, Borer NK, Stoia T, Atreya S. Integration concept for a hybrid-electric solid-oxide fuel cell power system into the X-57 'Maxwell. In: Proceedings of the 2018 Aviation Technology, Integration, and Operations Conference; 2018 Jun 25–29; Atlanta, GA, USA. Reston: American Institute of Aeronautics and Astronautics; 2018.
[31] Borer NK, Geuther SC, Litherland BL, Kohlman LW. Design and performance of a hybrid-electric fuel cell flight demonstration concept. In: Proceedings of the 2018 Aviation Technology, Integration, and Operations Conference; 2018 Jun 25–29; Atlanta, GA, USA. Reston: American Institute of Aeronautics and Astronautics; 2018. p. 3357.
[32] Cable TL, Setlock JA, Farmer SC, Eckel AJ. Regenerative performance of the NASA symmetrical solid oxide fuel cell design. Int J Appl Ceram Technol 2011;8(1):1–12.
[33] Veyo SE, Shockling LA, Dederer JT, Gillett JE, Lundberg WL. Tubular solid oxide fuel cell/gas turbine hybrid cycle power systems: status. J Eng Gas Turbine Power 2002;124(4):845–9.
[34] Kadhiresan AR, Duffy MJ. Conceptual design and mission analysis for eVTOL urban air mobility flight vehicle configurations. In: Proceedings of the AIAA Aviation 2019 Forum; 2019 Jun 17–21; Dallas, TX, USA. Reston: American Institute of Aeronautics and Astronautics; 2019.
[35] Kasliwal A, Furbush NJ, Gawron JH, McBride JR, Wallington TJ, De Kleine RD, et al. Role of flying cars in sustainable mobility. Nat Commun 2019;10(1):1555.
[36] Zheng C, Yan Y, Liu Y. Prospects of eVTOL and modular flying cars in China urban settings. J Intell Connect Veh 2023;6(4):187–9.
[37] Zhang J, Liu Y, Zheng Y. Overall eVTOL aircraft design for urban air mobility. Green Energy Intell Transport 2024;3(2):100150.
[38] Nizam Uddin Khan FM, Rasul MG, Sayem ASM, Mandal N. Maximizing energy density of lithium-ion batteries for electric vehicles: a critical review. Energy Rep 2023;9:11–21.[39] Qasem NAA, Abdulrahman GAQ. A recent comprehensive review of fuel cells: history, types, and applications. Int J Energy Res 2024;2024(1):7271748.

[40] Nicholas JD. Highlights from the 2013 national science foundation solid oxide fuel cell promise, progress, and priorities (SOFC-PPP) workshop. Elect
[41] Hesnmat H, Walton JF, Hunsberger A. Oil free 8 kW high-speed and high specific power turbogenerator. In: Proceedings of the ASME Turbo Expo 2014: Turbine Technical Conference and Exposition; 2014 Jun 16–20; Düsseldorf, Germany. New York City: The American Society of Mechanical Engineers; 2014. p. GT2014-27306, V01BT24A023.
[42] Picard B, Picard M, Plante J, Rancourt D. Optimum sub-megawatt electric-hybrid power source selection. Aircr Eng Aerosp Technol 2020;92(5):717–26.
[43] Courtin C, Mahseredjian A, Dewald AJ, Drela M, Hansman J. A performance comparison of eSTOL and eVTOL aircraft. In: Proceedings of the AIAA Aviation 2021 Forum; 2021 Aug 2–6; held virtually. Reston: American Institute of Aeronautics and Astronautics; 2021.
[44] Suri S. Novel and optimized techniques for storage and transportation of hydrogen: perspectives and challenges. J Appl Emerg Sci 2019;9(1):8.
[45] Qin L, Cheng Q, Mantzaras J, Law CK, Sui R. Surface-gas chemistry coupling and stability limits of hydrogen/air combustion in catalytic microchannels. Proc Combust Inst 2024;40(1–4):105229.
[46] Mantzaras J. Chapter three-catalytic combustion of hydrogen, challenges, and opportunities. Adv Chemical Eng 2014;45:97–157.
[47] Zhou Z, Lalwani AR, Sun X, Pan Z, Shahriary P, Xie Y, et al. Monolithic gyroidal solid oxide cells by additive manufacturing. Nat Energy 2025;10(8):962–70.
[48] Zhao B, Jian H, Qian Y, Zhuge W, Zhang Y, Zeng Z. Analyzing the thermal and electrical performance of a tubular SOFC with inserts by mass transfer coefficients. Appl Therm Eng 2024;242:122536.
[49] Zeng Z, Zhao B, Hao C, Essaghouri A, Qian Y, Zhuge W, et al. Effect of radial flows in fuel channels on thermal performance of counterflow tubular solid oxide fuel cells. Appl Therm Eng 2023;219:119577.
[50] Zhao B, Zeng Z, Hao C, Essaghouri A, Qian Y, Zhuge W, et al. A study of mass transfer characteristics of secondary flows in a tubular solid oxide fuel cell for power density improvement. Int J Energy Res 2022;46(13):18426–44.

Declaration of Interest Statement

☒ The authors declare that they have no known competing financial interests or personal relationships that could have appeared to influence the work reported in this paper.

☐ The author is an Editorial Board Member/Editor-in-Chief/Associate Editor/Guest Editor for this journal and was not involved in the editorial review or the decision to publish this article.

☐ The authors declare the following financial interests/personal relationships which may be considered as potential competing interests: